
Neural Sound Field Decomposition with Super-resolution of Sound Direction

Qiuqiang Kong¹, Shilei Liu¹, Junjie Shi¹, Xuzhou Ye¹
Yin Cao², Qiaoxi Zhu³, Yong Xu⁴, Yuxuan Wang¹

¹ ByteDance, Shanghai, China

² University of Surrey, Guildford, UK

³ University of Technology Sydney, Sydney, Australia

⁴ Tencent AI Lab, Bellevue, USA

¹{kongqiuqiang, liushilei.666, shijunjie, yexuzhou, wangyuxuan.11}@bytedance.com
²yin.cao@surrey.ac.uk, ³qiaoxi.zhu@uts.edu.au, ⁴lucayongxu@tencent.com

Abstract

Sound field decomposition predicts waveforms in arbitrary directions using signals from a limited number of microphones as inputs. Sound field decomposition is fundamental to downstream tasks, including source localization, source separation, and spatial audio reproduction. Conventional sound field decomposition methods such as Ambisonics have limited spatial decomposition resolution. This paper proposes a learning-based Neural Sound field Decomposition (NeSD) framework to allow sound field decomposition with fine spatial direction resolution, using recordings from microphone capsules of a few microphones at arbitrary positions. The inputs of a NeSD system include microphone signals, microphone positions, and queried directions. The outputs of a NeSD include the waveform and the presence probability of a queried position. We model the NeSD systems respectively with different neural networks, including fully connected, time delay, and recurrent neural networks. We show that the NeSD systems outperform conventional Ambisonics and DOANet methods in sound field decomposition and source localization on speech, music, and sound events datasets. Demos are available at¹.

1 Introduction

A sound field of a spatial region may contain sound waves propagating from different directions. Sound field decomposition [1–4] decomposes wave fields from arbitrary directions from signals recorded by microphone arrays. This work introduces a learning-based neural sound decomposition (NeSD) approach to predict *what*, *where*, and *when* are sound in a recording. The NeSD system can be used as pre-processing for downstream tasks, such as sound localization and direction of arrival estimation [5–10], sound event detection [11–13], source separation [14–18], beamforming [19–22], sound field reproduction [23–25], and augmented reality (AR) and virtual reality (VR) [26–28].

A sound field consists of sounds coming from different directions. For example, musicians in a band may have different locations on a stage. Multiple speakers may have different locations in a room. Sound localization [6], also called direction of arrival (DOA) estimation, is a task to predict the locations of sources. Previous DOA methods include parametric-based methods such as time difference of arrival (TDOA) [29] and multiple signal classification (MUSIC) [30]. Recently, neural networks have been introduced to address the DOA problem, such as convolutional recurrent neural networks (CRNNs) [5, 8] and two stages estimation methods [7]. However, many conventional DOA

¹<https://www.youtube.com/watch?v=0GIr6doj3BQ>

methods require the number of microphones to be larger than the number of sources and can not decompose waveforms.

Another challenge of sound field decomposition is to separate signals in the sound field from different directions. Beamforming [31, 32, 21, 22] is a technique to filter signals in specific beams. Conventional beamforming methods include the minimum variance distortionless response (MVDR) [33]. Recently, neural network-based beamforming methods have been proposed for beamforming [21, 22]. However, those beamforming methods do not predict the localization of sources. Previous neural network-based beamforming methods focused on on speech and were not train on the general sound sounds. Sound field decomposition is also related to the source separation problem, where deep neural networks have been applied to address the source separation problem [18, 14, 34, 35, 15]. However, many source separation systems do not separate correlated waveforms from different directions. Recently, unsupervised source separation methods [36–38] were proposed to separate unseen sources. Still, those methods do not separate highly correlated sources and do not predict the directions of sources.

The conventional way of sound field decomposition requires numerous measurements to capture a sound field. First-order Ambisonics (FOA) [39–41] and high-order Ambisonics (HOA) [42, 43] were proposed to record sound fields. Ambisonics provides truncated spherical harmonic decomposition of a sound field. A K -th order ambisonics require $(K + 1)^2$ channels to record a sound field. A sound field is hard to record and process when K is large. Moreover, the accurate reproduction in a head-sized volume up to 20 kHz would require an order K of more than 30. Recently, DOANet [44] was proposed to predict pseudo-spectrum, while does not predict waveforms. Still, here is a lack of works on neural network-based sound field decomposition that can achieve super-resolution of a sound field.

In this work, we propose a NeSD framework to address the sound field decomposition problem. The NeSD approach is inspired by the neural radiance fields (NeRF) [45] for view synthesis in computer vision. NeSD has the advantage of predicting the locations of wideband, non-stationary, moving, and arbitrary number of sources in a sound field. NeSD supports any layout of microphone array types, including uniform or non-uniform arrays such as planar, spherical array, or other irregular arrays. NeSD also supports the microphones to have different directivity patterns. NeSD can separate correlated signals in a sound field. NeSD can decompose a sound field with arbitrary spatial resolutions and can achieve better directivity than FOA and HOA methods. In training, the inputs to a NeSD system include the signals of arbitrary microphone arrays, the positions of all microphones, and arbitrary queried directions on a sphere. In inference, all sound field directions are input to the trained NeSD in mini-batches to predict the waveforms and the presence probabilities of sources in a sound field.

This work is organized as follows. Section 2 introduces the sound field decomposition problem. Section 3 introduces our proposed NeSD framework. Section 4 shows experiments. Section 5 concludes this work.

2 Problem Statement

The signals recorded from a microphone capsule are denoted as $\mathbf{x} = \{x_1(t), \dots, x_M(t)\}$, where M is the number of microphones in the capsule. The m -th microphone signal is $x_m(t) \in \mathbb{R}^T$ where T is the number of samples in an audio segment. The microphone capsule can be any type, such as the Ambisonics or circular capsule.

The coordinate of the m -th microphone in the spherical coordinate system is $q_m(t)$, where $q_m(t) = \{r_m(t), \theta_m(t), \phi_m(t)\}$ denotes the distance, azimuthal angle, and polar angle of the microphone. The position information of all microphones is $\mathbf{q} = \{q_1(t), \dots, q_M(t)\}$. Note that $q_m(t)$ is a time-dependent variable to reflect moving microphones. For a static microphone, all of $r_m(t)$, $\theta_m(t)$, and $\phi_m(t)$ in $q_m(t)$ have constant values.

We denote a continuous sound field as $\mathbf{s} = s(\Omega, t) \in \mathbb{S}^2 \times \mathbb{R}^T$ where \mathbb{S}^2 is a sphere. Each direction Ω is described by an azimuth angle $\theta \in [0, 2\pi)$ and a polar angle $\phi \in [0, \pi]$. Sound field decomposition is a task to estimate \mathbf{s} from the microphone signals \mathbf{x} and the microphone positions \mathbf{q} :

$$\hat{s}(\Omega, t) = f_{\mathbb{S}^2}(\mathbf{x}, \mathbf{q}), \quad (1)$$

where $f_{\mathbb{S}^2}(\cdot, \cdot)$ is a sound field decomposition mapping and $\hat{s}(\Omega, t)$ is the estimated waveform.

3 Neural Sound Field Decomposition (NeSD)

We introduce the training, the data creation, the NeSD architecture, the hard example mining, and the inference of NeSD in this section.

3.1 Empirical Risk

Directly model $f_{\mathbb{S}^2}$ is intractable because the output dimension $\mathbb{S}^2 \times \mathbb{R}^L$ is infinite. Instead, we propose a mapping f to predict $\hat{s}(\Omega, t)$ conditioned on a direction Ω for all $\Omega \in \mathbb{S}^2$:

$$\hat{s}(\Omega, t) = f(\mathbf{x}, \mathbf{q}, \Omega), \quad (2)$$

We model f in (2) by using a neural network. We denote the risk l between the estimated sound field \hat{s} and the oracle sound field s as:

$$l = \mathbb{E}_{\mathbf{s} \sim p_{\text{field}}(\mathbf{s})} \mathbb{E}_{\Omega \sim p_{\text{sphere}}(\Omega)} \mathbb{E}_{t \sim p_{\text{time}}(t)} d(s(\Omega, t), \hat{s}(\Omega, t)), \quad (3)$$

where p_{field} , p_{sphere} , and p_{time} are the distributions of sound field \mathbf{s} , direction Ω , and time t , respectively. The loss function is denoted by $d(\cdot, \cdot)$. Equation (3) shows that the risk l consists of expectations over p_{field} , p_{sphere} , and p_{time} . However, directly optimize the risk (3) is intractable. To address this problem, we propose to minimize the empirical risk in mini-batches:

$$l_{\text{batch}} = \sum_{b=1}^B \sum_{\substack{\Omega \sim p_{\text{sphere}}(\Omega) \\ q=1}}^Q \sum_{t=1}^T d(s(\Omega, t), \hat{s}(\Omega, t)), \quad (4)$$

where B is the mini-batches number to sample sound fields from a dataset and Q is the number of directions to sample on a sphere. In each mini-batch, sound field signals \mathbf{s} are sampled from $p_{\text{field}}(\mathbf{s})$. Directions Ω are sampled from $p_{\text{sphere}}(\Omega)$. By this means, the optimization of (4) is tractable. The risk (4) is differentiable with respect to the learnable parameters of f , so that the learnable parameters can be optimized by gradient-based methods.

3.2 Create Microphone Sound Field Signals

The optimization of (4) requires paired microphone signals \mathbf{x} , microphone positions information \mathbf{q} and sound field signals \mathbf{s} for training. However, it is impossible to obtain oracle sound field signals \mathbf{s} in real scenes. To address this problem, we propose to create microphone and sound field signals from point sources.

We create I far field point sources $\{a_i(t)\}_{i=1}^I$ from I randomly sampled directions $\{\Omega_i\}_{i=1}^I$. Each $a_i(t)$ is a randomly selected monophonic audio segment from an audio dataset such as a speech or a music dataset. In a free field without room reverberation, the sound field \mathbf{s} can be created by:

$$s(\Omega, t) = \begin{cases} a_i(t), & \Omega = \Omega_i \\ 0, & \Omega \in \mathbb{S}^2 / \{\Omega_i\}_{i=1}^I \end{cases} \quad (5)$$

In (5), a sound field \mathbf{s} only has non-zero values in the directions containing point sources.

Next, we create microphone signals \mathbf{x} . First, all I point source signals are propagated to all M microphones. We denote $a_{i,m}^{(\text{delay})}(t)$ as the i -th point source signal arrives the m -th microphone:

$$a_{i,m}^{(\text{delay})}(t) = a_i(t - \tau_{i,m}), \quad (6)$$

where $\tau_{i,m}$ is the propagation time as shown in Fig. 1. The propagation time $\tau_{i,m}$ can be calculated by the speed of sound c , the distance from the m -th microphone to the origin r_m , and the included angle Ω_Δ between the i -th point source and the m -th microphone by: $\tau_{i,m} = -r_m \cos \Omega_\Delta$ as shown in Fig. 1.

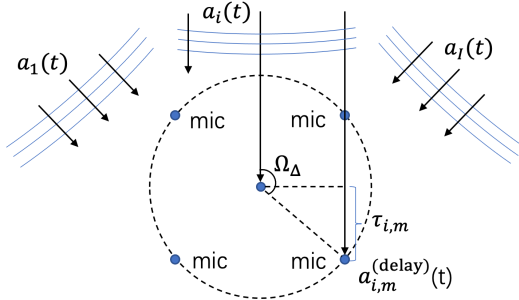


Figure 1: Point source signals arrive microphones.

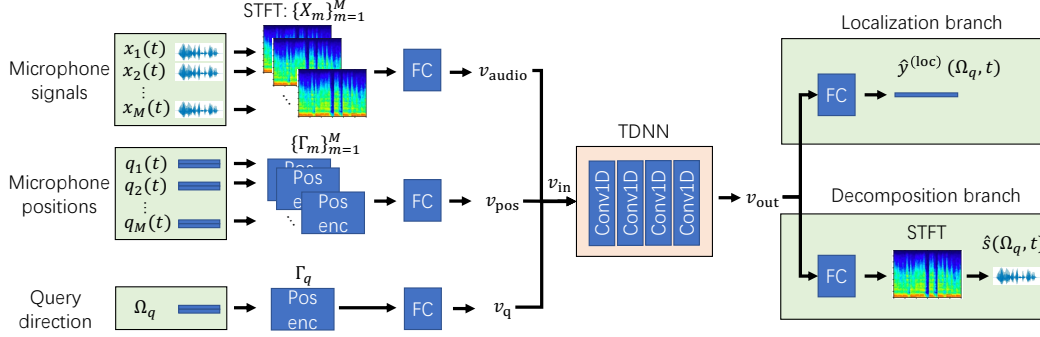


Figure 2: Framework of the NeSD system.

Microphones have different directivity patterns. So the signal recorded by a microphone can be different from the signal arrives the microphone. We denote the i -th signal recorded by the m -th microphone as:

$$a_{i,m}^{(\text{mic})}(t) = g(a_{i,m}^{(\text{delay})}(t), \Omega_{\Delta}), \quad (7)$$

where g is a transfer function. To simplify g , we assume the directivity pattern is constant for all frequencies. Then, equation (7) equals $a_{i,m}^{(\text{delay})}(t)$ for an omni microphone and equals $a_{i,m}^{(\text{delay})}(t)(1 + \cos \Omega_{\Delta})/2$ for a cardioid microphone. Then, the microphone signals of all point sources $a_{i,m}^{(\text{mic})}(t)$ are summed to constitute the m -th microphone signal:

$$x_m(t) = \sum_{i=1}^I a_{i,m}^{(\text{mic})}(t) \quad (8)$$

The microphone positions information \mathbf{q} can be obtained from the pre-defined microphone array. By this means, we obtain paired \mathbf{x} , \mathbf{q} , and \mathbf{s} to train the NeSD system.

3.3 NeSD Input Embeddings

The core part of a NeSD system is to build the mapping in (2). The input to a NeSD system includes the microphone signals \mathbf{x} , the microphone positions information \mathbf{q} , and queried directions Ω_q . Fig. 2 shows the NeSD framework. We describe the submodules of a NeSD system as follows.

3.3.1 Audio Embedding

We apply short-time Fourier transform (STFT) on each microphone signal $x_m(t)$ to extract the STFT of waveforms. Each STFT X_m has a shape of $L \times F$, where L and F are frames number and frequency bins number, respectively. We concatenate M STFTs $\{X_m\}_{m=1}^M$ along the frequency axis to constitute X_{concat} with a shape of $L \times FM$. Then, we apply a fully connected layer on X_{concat} to calculate an *audio embedding* v_{audio} with a shape of $L \times C$:

$$v_{\text{audio}} = X_{\text{concat}}W_{\text{audio}} + b_{\text{audio}}, \quad (9)$$

where C is the hidden units number. W_{audio} and b_{audio} are learnable weights and biases with shapes of $MF \times C$ and C , respectively. The audio embedding v_{audio} contains the content information of microphone signals.

3.3.2 Microphone Positions Embedding

We map the microphone positions to a *microphone positions embedding* v_{pos} which contains the position information of all microphones. We find that directly construct v_{pos} from $\theta_m(t)$ and $\phi_m(t)$ leads to poor performance in sound field decomposition. To address this problem, we propose to apply positional encoding [45] on $\theta_m(t)$ and $\phi_m(t)$:

$$\begin{aligned} \gamma(\theta) &= \{\sin(2^0\pi\theta), \cos(2^0\pi\theta), \dots, \sin(2^{P-1}\pi\theta), \cos(2^{P-1}\pi\theta)\} \\ \gamma(\phi) &= \{\sin(2^0\pi\phi), \cos(2^0\pi\phi), \dots, \sin(2^{P-1}\pi\phi), \cos(2^{P-1}\pi\phi)\}, \end{aligned} \quad (10)$$

where the subscript m and t are omitted for (10) for conciseness and P is a hyper-parameter. Larger P indicates better spatial resolution. Positional encodings have the advantage of remaining high frequency of spatial angles and is beneficial for high-resolution sound field decomposition. We denote the position encoding of the m -th microphone as $\Gamma_m = \{\gamma(\theta), \gamma(\phi)\}$ with a shape of $L \times 4P$, where the number 4 includes the cosine and sine of the azimuth angle and polar angle. We concatenate all M position encodings along the feature dimension to obtain Γ_{concat} which has a shape of $L \times 4PM$. Then, we apply a fully connected layer on Γ_{concat} to calculate a microphone positions embedding v_{pos} with a shape of $L \times C$:

$$v_{\text{pos}} = \Gamma_{\text{concat}}W_{\text{pos}} + b_{\text{pos}}, \quad (11)$$

where W_{pos} and b_{pos} are learnable weights and bias with shapes of $4MP \times C$ and C , respectively.

3.3.3 Query Direction Embedding

A query direction Ω_q is used to condition a NeSD in (2) to predict the decomposed waveform $\hat{s}(\Omega_q, t)$ in direction Ω_q . Similar to the microphone position encoding in (10), we map Ω_q to a position embedding Γ_q with a shape of $L \times 4P$. Then, we apply a fully connected layer on Γ_q to calculate a *query direction embedding* v_q with a shape of $L \times C$:

$$v_q = \Gamma_qW_q + b_q, \quad (12)$$

where W_q and b_q are learnable weights and bias with shapes of $4P \times C$ and C , respectively. The query direction embedding v_q contains high spatial resolution information of the query direction Ω_q .

Then, we concatenate all the audio embedding v_{audio} , the microphone positions embedding v_{pos} , and the query direction embedding v_q along the feature dimension to calculate an input embedding v_{in} with a shape of $T \times 3C$. The input embedding v_{in} contains all information of microphone signals, the microphone positions, and query directions.

3.4 NeSD Backbone Networks

We apply a time delay neural network (TDNN) [46] on v_{in} to extract the high-level information of microphone signals, microphone positions, and query directions. The TDNN consists of four time-domain one-dimensional convolutional layers. Each convolutional layer outputs H channels followed by a batch normalisation [47] and a ReLU non-linearity [48]. A TDNN has the advantage of capturing time-dependent information. In a special case when the kernel sizes of convolutional layers are set to 1, the convolutional layers are reduced to fully connected layers. We denote the output of the backbone network is as v_{out} with a shape of $T \times H$. In addition, we implement a 3-layer fully connected neural network and a 3-layer bi-directional gated recurrent unit (GRU) [49] as backbone networks for comparison.

3.5 NeSD Output Branches

We build multiple output branches on the backbone network output v_{out} to support multiple tasks, including sound localization and decomposition.

3.5.1 Sound Localization Branch

In the sound localization branch shown in Fig. 2, we apply a fully connected layer on v_{out} followed by a sigmoid nonlinearity to predict the presence probability of sources in direction Ω_q :

$$\hat{y}_{\text{loc}}(\Omega_q, n) = \sigma(v_{\text{out}}V_{\text{loc}} + b_{\text{loc}}), \quad (13)$$

where n is the frame index, and V_{loc} and b_{loc} are learnable weights and biases with shapes of $C \times 1$ and 1, respectively. The output probability $\hat{y}_{\text{loc}}(\Omega_q, n)$ indicates the probability of point sources in direction Ω_q .

3.5.2 Source Decomposition Branch

In the source decomposition branch shown in Fig. 2, we apply a fully connected layer on v_{out} followed by a sigmoid nonlinearity to predict the ideal ratio mask [50] of the input omni waveform in the

Algorithm 1 Hard example mining of one query direction.

Inputs: \mathbb{S}^2 , point source directions $\{\Omega_i\}_{i=1}^I$, $p_{\text{thres}} = 0.9$.
Outputs: a query direction Ω_q .
 Sample $p \sim \text{Uniform}(0, 1)$
if $p < p_{\text{thres}}$ **then**
 Sample $\Omega_q \sim \mathbb{S}^2$.
else
 Sample $\Omega_q \sim \{\Omega\}_{i=1}^I$.
end if

time-frequency domain, where the omni waveform is calculated by averaging all microphone signals. The time-frequency mask in direction Ω_q is predicted by:

$$M(\Omega_q, n, f) = \sigma(v_{\text{out}}V_{\text{ss}} + b_{\text{ss}}), \quad (14)$$

where n and f are frame index and frequency bin index, respectively. Matrices V_{ss} and b_{ss} are learnable weights and biases with shapes of $C \times 1$ and 1 , respectively. The time-frequency mask $M(\Omega_q, n, f)$ has a shape of $T \times F$ and is multiplied with the STFT of the omni waveform $X_{\text{omni}}(n, f)$ followed by an inverse STFT to obtain the separated waveform $\hat{s}(\Omega_q, t)$ at Ω_q :

$$\hat{s}(\Omega_q, t) = \mathcal{F}^{-1}(M(\Omega_q, n, f) \odot X_{\text{omni}}(n, f)), \quad (15)$$

where \mathcal{F}^{-1} is the inverse STFT, and \odot is the element-wise multiplication.

3.6 Loss Function

The loss function d in (4) consists of a localization loss l_{loc} and a decomposition loss l_{ss} :

$$d = l_{\text{loc}} + l_{\text{ss}}, \quad (16)$$

where l_{loc} is the binary cross-entropy between the predicted presence probability $\hat{y}_{\text{loc}}(\Omega_q, n)$ and the ground truth $y_{\text{loc}}(\Omega_q, n)$ in a queried direction Ω_q :

$$l_{\text{loc}} = l_{\text{bce}}(\hat{y}_{\text{loc}}(\Omega_q, n), y_{\text{loc}}(\Omega_q, n)) \quad (17)$$

The source decomposition loss is the mean absolute error between the predicted waveform $\hat{s}(\Omega_q, t)$ and the ground truth waveform $s(\Omega_q, t)$ in a queried direction Ω_q :

$$l_{\text{ss}} = \|\hat{s}(\Omega_q, t) - s(\Omega_q, t)\|_1, \quad (18)$$

3.7 Hard Example Mining

The empirical loss (4) requires the sampling of \mathbf{s} from $p_{\text{field}}(\mathbf{s})$ and the sampling of query directions Ω_q from $p_{\text{sphere}}(\Omega)$. On one hand, we uniformly sample audio segments $a_i(t)$ from an audio dataset and process $a_i(t)$ to \mathbf{s} by (5). On the other hand, we need to elaborately sample query directions Ω_q to avoid the situation where all query directions are silent. We propose a hard mining strategy in Algorithm 1 to increase the proportion of non-silent query directions among Q sampled directions. Fig. 3 shows an example of Q sampled query directions by Algorithm 1. The cross symbols are sampled query directions. The red dots are the positions of point sources.

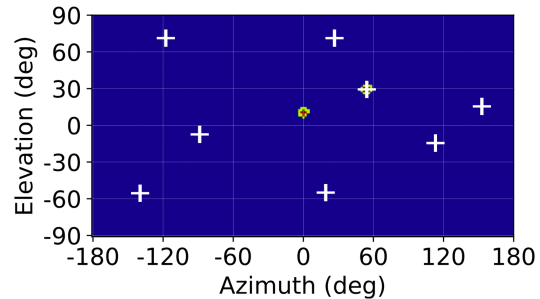


Figure 3: The cross symbols show the sampled query directions by using Algorithm 1.

3.8 Inference

Algorithm 2 summarizes the training of a NeSD system. At inference, we input the microphone signals \mathbf{x} , the microphone positions information \mathbf{q} , and any query directions Ω_q to the trained NeSD

Algorithm 2 Training of a NeSD system.

- 1: **Inputs:** An audio dataset \mathbb{D} . Microphone positions \mathbf{q} . B : mini-batch size, I : sources number, Q : query directions number.
 - 2: **Outputs:** Optimized parameters of a NeSD system.
 - 3: **while** not converge **do**
 - 4: **for** $b = 1, \dots, B$ **do**
 - 5: Sample $\{a_i(t)\}_{i=1}^I$ uniformly from \mathbb{D} .
 - 6: Constitute \mathbf{s} by using (5) and \mathbf{x} by using (8).
 - 7: **for** $q = 1, \dots, Q$ **do**
 - 8: Sample a query direction Ω_q by using Algorithm 1.
 - 9: **end for**
 - 10: Constitute the b -th training data: $\{\mathbf{x}, \mathbf{q}, \{\Omega_q\}_{q=1}^Q\}$
 - 11: **end for**
 - 12: Calculate empirical loss by (4) and (16). Calculate the gradient with respect to the learnable parameters of NeSD.
 - 13: Update the learnable parameters with gradient-based optimization methods.
 - 14: **end while**
-

Algorithm 3 Sound field decomposition with a trained NeSD system.

- 1: **Inputs:** \mathbf{x}, \mathbf{q} .
 - 2: **Outputs:** \mathbf{s}
 - 3: **for** $\Omega \in \mathbb{S}^2$ **do**
 - 4: $\hat{\mathbf{s}}(\Omega, t) = f(\mathbf{x}, \mathbf{q}, \Omega)$
 - 5: **end for**
-

system. For the sound field decomposition purpose, we input all azimuth angle and polar angle combinations to the NeSD system. The azimuth angles and polar angles have a granularity of κ degrees. The granularity κ can be tuned in the inference stage. Lower κ leads to higher spatial decomposition resolution while requires higher computation cost. Algorithm 3 summarizes the inference of a NeSD system.

4 Experiments

4.1 Datasets

We experiment the NeSD system across a variety of datasets including speech, music, and sound events datasets. We apply the VCTK dataset [51] containing 108 speakers as the speech dataset. The VCTK dataset is split into 100 speakers for training and 8 speakers for testing. We apply the MUSDB18 dataset [52] containing 150 songs as the music dataset. The MUSDB18 dataset is split into 100 songs for training and 50 songs for testing. Each song contains four individual tracks including vocals, bass, drums, and other. We apply the NIGENS dataset [53] containing 14 distinguished sound classes as the sound events dataset.

We resample all audio recordings into 16 kHz and remove all silent frames. Then, audio recordings are split into 3-second segments. We apply a STFT with a window size of 32 ms and a hop size of 10 ms to calculate audio embeddings as described in Section 3.3.1. We set the position encoding hyper-parameter P described in (10) to 5. The hidden units C is set to 128 and the number of output feature maps number H is set to 256. An Adam optimizer [54] with a learning rate of 0.001 is used to train the NeSD system. The training takes 6 hours on a single Tesla V100 GPU card.

4.2 Sound Field Energy

First, we apply the mean absolute error between the predicted sound field energy and the ground truth sound field energy to evaluate the sound field decomposition performance:

$$MAE = \frac{1}{\sum_{\Omega \in \mathbb{S}^2} N} \sum_{\Omega \in \mathbb{S}^2} \sum_{n=1}^N |\hat{y}_{\text{loc}}(\Omega, n) - y_{\text{loc}}(\Omega, n)| \quad (19)$$

Table 1: Mean absolute error of sound field field decomposition.

| | mic. | SPEECH | | | | MUSIC | | | | SOUND EVENT | | | |
|--------------|------|--------------|--------------|--------------|--------------|--------------|--------------|--------------|--------------|--------------|--------------|--------------|--------------|
| | | 1 src | 2 src | 4 src | 8 src | 1 src | 2 src | 4 src | 8 src | 1 src | 2 src | 4 src | 8 src |
| Ambisonics 1 | 4 | 0.454 | 0.673 | 0.984 | 1.775 | 0.428 | 0.649 | 1.117 | 1.633 | 0.489 | 0.493 | 0.962 | 2.000 |
| Ambisonics 3 | 16 | 0.188 | 0.271 | 0.401 | 0.778 | 0.168 | 0.267 | 0.470 | 0.679 | 0.214 | 0.300 | 0.451 | 0.768 |
| NeSD-DNN | 4 | 0.095 | 0.240 | 0.314 | 0.372 | 0.075 | 0.258 | 0.295 | 0.328 | 0.094 | 0.278 | 0.294 | 0.313 |
| NeSD-TDNN | 4 | 0.020 | 0.045 | 0.103 | 0.233 | 0.016 | 0.070 | 0.172 | 0.250 | 0.021 | 0.113 | 0.217 | 0.266 |
| NeSD-GRU | 4 | 0.011 | 0.017 | 0.046 | 0.114 | 0.012 | 0.042 | 0.117 | 0.154 | 0.013 | 0.067 | 0.155 | 0.214 |

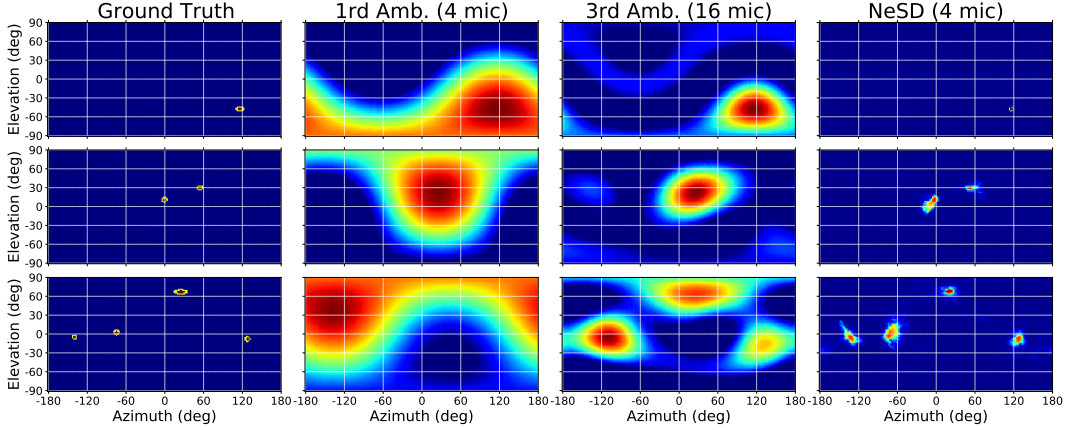


Figure 4: Sound field decomposition. From left to right: ground truth sound field containing one to four speakers, sound field decomposition with 1-order Ambisonics, with 3-order Ambisonics, and with NeSD.

Table 1 shows the comparison of using Ambisonics methods and the NeSD methods to decompose sound fields. We experiment on sound fields containing 1, 2, 4, and 8 sources. The source types vary from speech, music, to sound events. Lower MAE indicates better performance. Table 1 shows that all our proposed NeSD-DNN, NeSD-TDNN, and NeSD-GRU systems achieve lower MAE than Ambisonics-based methods. Specifically, the NeSD-GRU system achieves lower MAE than the NeSD-DNN and the NeSD-TDNN system, indicating that long-time dependency is beneficial for audio localization. The NeSD systems with 4 microphones even surpass the 3-order Ambisonics system recorded with 16 microphones. The first column in Fig. 4 shows the ground truth sound field. The second and third column show the 1-order and 3-order decomposition results. The fourth row shows the sound field predicted by NeSD. Fig. 4 shows that the NeSD system achieves a better estimation of the ground truth sound field than Ambisonics decoding. The NeSD-GRU system achieves an MAE of 0.011 to 0.114 from 1 source to 8 sources evaluated on speech, compared with the 3-order Ambisonic method from 0.188 to 0.778.

4.3 Sound Field Decomposition

We apply the signal-to-distortion for decomposition (SDRD) metric [3] to evaluate sound field decomposition. Different from conventional source decomposition metrics, SDRD evaluate the SDR in the entire sound field.

$$SDRD = 10 \log_{10} \frac{\sum_{\Omega \in \mathbb{S}^2} \sum_{t=1}^T |s(\Omega, t)|^2}{\sum_{\Omega \in \mathbb{S}^2} \sum_{t=1}^T |s(\Omega, t) - \hat{s}(\Omega, t)|^2} \quad (20)$$

Table 2 shows the comparison of SDRD using Ambisonics methods and the NeSD methods to decompose sound fields. The higher SDRD indicates the better performance. The 0-order Ambisonics is regarded as a baseline system which indicates no decomposition. The 0-order Ambisonics achieves SDRD of around -30 dB. Table 2 shows that the NeSD systems significantly improve the Ambisonics methods by 20 to 30 dB. The NeSD-TDNN system and the NeSD-GRU system achieve similar

Table 2: SDRD results (dB)

| | mic. | SPEECH | | | | MUSIC | | | | SOUND EVENT | | | |
|--------------|------|--------------|--------------|--------------|--------------|--------------|---------------|---------------|--------------|--------------|--------------|---------------|---------------|
| | | 1 src | 2 src | 4 src | 8 src | 1 src | 2 src | 4 src | 8 src | 1 src | 2 src | 4 src | 8 src |
| Ambisonics 0 | 1 | -33.68 | -32.41 | -33.55 | -32.12 | -33.64 | -33.11 | -29.37 | -31.59 | -30.17 | -30.88 | -32.04 | -32.93 |
| Ambisonics 1 | 4 | -27.78 | -27.20 | -27.43 | -26.70 | -27.20 | -27.57 | -24.34 | -26.27 | -25.49 | -26.09 | -26.88 | -27.09 |
| Ambisonics 3 | 16 | -22.00 | -21.62 | -21.15 | -21.31 | -21.25 | -21.66 | -19.43 | -20.81 | -20.73 | -20.95 | -21.49 | -21.46 |
| NeSD-DNN | 4 | -2.86 | -10.55 | -11.91 | -9.34 | -5.45 | -12.78 | -13.00 | -10.32 | -2.91 | -11.21 | -12.29 | -11.38 |
| NeSD-TDNN | 4 | -1.66 | -4.84 | -7.14 | -6.77 | -3.96 | -11.29 | -11.87 | -9.45 | -1.32 | -9.14 | -12.13 | -10.81 |
| NeSD-GRU | 4 | -0.80 | -6.11 | -6.78 | -4.67 | -3.82 | -14.39 | -13.74 | -9.67 | -3.27 | -14.16 | -13.00 | -11.44 |

Table 3: DOA results (degree)

| | mic. | SPEECH | | | | MUSIC | | | | SOUND EVENT | | | |
|-------------|------|--------|-------|-------|-------|-------|-------|-------|-------|-------------|-------|-------|-------|
| | | 1 src | 2 src | 4 src | 8 src | 1 src | 2 src | 4 src | 8 src | 1 src | 2 src | 4 src | 8 src |
| DOANet [44] | 4 | 6.69 | 9.40 | 19.36 | 22.11 | 7.23 | 24.52 | 21.71 | 26.92 | 11.39 | 30.96 | 31.37 | 22.40 |
| NeSD-DNN | 4 | 1.31 | 6.09 | 12.52 | 17.33 | 2.03 | 7.50 | 14.83 | 19.70 | 2.64 | 13.36 | 22.21 | 23.48 |
| NeSD-TDNN | 4 | 0.91 | 1.93 | 4.22 | 8.49 | 1.51 | 3.70 | 8.29 | 14.44 | 1.57 | 6.50 | 16.05 | 20.68 |
| NeSD-GRU | 4 | 1.01 | 1.70 | 4.12 | 7.46 | 1.52 | 7.66 | 13.04 | 18.21 | 1.48 | 11.69 | 22.56 | 23.73 |

results, both of which outperform the NeSD-DNN system, indicating that temporal information is important for sound field decomposition.

4.4 Source Localization

We evaluate the average angular error E_{DOA} in degrees between the ground truth direction and the predicted direction of sources as the source localization metric [44]. Lower DOA_{error} indicates better performance. We apply the DOANet [44] as the baseline system. The evaluation metric is the averaged DOA error over frames:

$$E_{\text{DOA}} = \frac{1}{NI} \sum_{n=1}^N \sum_{i=1}^I |\hat{\Omega}_{n,i}^{(\text{DOA})} - \Omega_{n,i}^{(\text{DOA})}| \quad (21)$$

where $\hat{\Omega}_{n,i}^{(\text{DOA})}$ and $\Omega_{n,i}^{(\text{DOA})}$ are the estimated and the ground truth DOA in the n -th frame, respectively. The estimated DOA $\hat{\Omega}_{n,i}^{(\text{DOA})}$ is calculated simply by selecting directions with local maximum values on the estimated sound field. Table 3 shows that all of NeSD-DNN, NeSD-TDNN, and NeSD-GRU systems outperform the DOANet. The NeSD-TDNN system achieves a DOA error of 0.91 degrees compared with the DOANet of 6.69 degrees in one source speech localization. The DOA error increases with the number of sources in all systems. Both the NeSD-TDNN and the NeSD-GRU systems achieve similar results and outperform the NeSD-DNN system, indicating that the temporal information of sources are important for source localization.

5 Conclusion

We propose a learning-based neural sound field decomposition (NeSD) framework to address the sound field decomposition problem with limited number of microphones. NeSD allow sound field decomposition with fine sound direction resolution. The inputs of a NeSD system include microphone signals, microphone positions, and queried directions. The decomposed sound field can be calculated by input arbitrary query directions to the trained NeSD system. The NeSD system can be used to predict what, where, and when are sound sources by using a unified framework. We show the the NeSD method outperforms Ambisonic and DOANet systems on wideband and mutiple sources speech, music, and sound events datasets. In future, we will explore NeSD for downstream tasks, including source localization, multiple source separation, moving object detection, and sound field reproduction tasks.

References

- [1] Rafaely, B. Plane-wave decomposition of the sound field on a sphere by spherical convolution. *The Journal of the Acoustical Society of America*, 116(4):2149–2157, 2004.
- [2] Bernschütz, B. *Microphone arrays and sound field decomposition for dynamic binaural recording*. Technische Universitaet Berlin, 2016.
- [3] Koyama, S., N. Murata, H. Saruwatari. Sparse sound field decomposition for super-resolution in recording and reproduction. *The Journal of the Acoustical Society of America*, 143(6):3780–3795, 2018.
- [4] Zhu, Q., X. Qiu, P. Coleman, et al. An experimental study on transfer function estimation using acoustic modelling and singular value decomposition. *The Journal of the Acoustical Society of America*, 150(5):3557–3568, 2021.
- [5] Adavanne, S., A. Politis, J. Nikunen, et al. Sound event localization and detection of overlapping sources using convolutional recurrent neural networks. *IEEE Journal of Selected Topics in Signal Processing*, 13(1):34–48, 2018.
- [6] Politis, A., A. Mesaros, S. Adavanne, et al. Overview and evaluation of sound event localization and detection in dcase 2019. *IEEE/ACM Transactions on Audio, Speech, and Language Processing*, 29:684–698, 2020.
- [7] Cao, Y., T. Iqbal, Q. Kong, et al. Two-stage sound event localization and detection using intensity vector and generalized cross-correlation. *Tech. report of Detection and Classification of Acoustic Scenes and Events (DCASE) Challenge*, 2019.
- [8] Grondin, F., J. Glass, I. Sobieraj, et al. Sound event localization and detection using CRNN on pairs of microphones. In *Detection and Classification of Acoustic Scenes and Events (DCASE) Technique Report*. 2019.
- [9] Qin, S., Y. D. Zhang, M. G. Amin. Generalized coprime array configurations for direction-of-arrival estimation. *IEEE Transactions on Signal Processing*, 63(6):1377–1390, 2015.
- [10] Xiao, X., S. Zhao, X. Zhong, et al. A learning-based approach to direction of arrival estimation in noisy and reverberant environments. In *IEEE International Conference on Acoustics, Speech and Signal Processing (ICASSP)*, pages 2814–2818. 2015.
- [11] Mesaros, A., T. Heittola, T. Virtanen. Tut database for acoustic scene classification and sound event detection. In *IEEE European Signal Processing Conference (EUSIPCO)*, pages 1128–1132. 2016.
- [12] Cakır, E., G. Parascandolo, T. Heittola, et al. Convolutional recurrent neural networks for polyphonic sound event detection. *IEEE/ACM Transactions on Audio, Speech, and Language Processing*, 25(6):1291–1303, 2017.
- [13] Kong, Q., Y. Cao, T. Iqbal, et al. Panns: Large-scale pretrained audio neural networks for audio pattern recognition. *IEEE/ACM Transactions on Audio, Speech, and Language Processing*, 28:2880–2894, 2020.
- [14] Stöter, F.-R., S. Uhlich, A. Liutkus, et al. Open-unmix-a reference implementation for music source separation. *Journal of Open Source Software*, 4(41):1667, 2019.
- [15] Défossez, A., N. Usunier, L. Bottou, et al. Music source separation in the waveform domain. *arXiv preprint arXiv:1911.13254*, 2019.
- [16] Seetharaman, P., G. Wichern, S. Venkataramani, et al. Class-conditional embeddings for music source separation. In *IEEE International Conference on Acoustics, Speech and Signal Processing (ICASSP)*, pages 301–305. 2019.
- [17] Xu, Y., J. Du, L.-R. Dai, et al. An experimental study on speech enhancement based on deep neural networks. *IEEE Signal processing letters*, 21(1):65–68, 2013.

- [18] Luo, Y., N. Mesgarani. Conv-TasNet: Surpassing ideal time–frequency magnitude masking for speech separation. *IEEE/ACM Transactions on Audio, Speech, and Language Processing*, 27(8):1256–1266, 2019.
- [19] Huang, H., Y. Peng, J. Yang, et al. Fast beamforming design via deep learning. *IEEE Transactions on Vehicular Technology*, 69(1):1065–1069, 2019.
- [20] Alkhateeb, A., S. Alex, P. Varkey, et al. Deep learning coordinated beamforming for highly-mobile millimeter wave systems. *IEEE Access*, 6:37328–37348, 2018.
- [21] Xu, Y., M. Yu, S.-X. Zhang, et al. Neural spatio-temporal beamformer for target speech separation. In *INTERSPEECH*. 2020.
- [22] Zhang, Z., Y. Xu, M. Yu, et al. Adl-mvdr: All deep learning mvdr beamformer for target speech separation. In *IEEE International Conference on Acoustics, Speech and Signal Processing (ICASSP)*, pages 6089–6093. 2021.
- [23] Betlehem, T., T. D. Abhayapala. Theory and design of sound field reproduction in reverberant rooms. *The Journal of the Acoustical Society of America*, 117(4):2100–2111, 2005.
- [24] Donley, J., C. Ritz, W. B. Kleijn. Multizone soundfield reproduction with privacy-and quality-based speech masking filters. *IEEE/ACM Transactions on Audio, Speech, and Language Processing*, 26(6):1041–1055, 2018.
- [25] Han, Z., M. Wu, Q. Zhu, et al. Two-dimensional multizone sound field reproduction using a wave-domain method. *The Journal of the Acoustical Society of America*, 144(3):EL185–EL190, 2018.
- [26] Vorländer, M., D. Schröder, S. Pelzer, et al. Virtual reality for architectural acoustics. *Journal of Building Performance Simulation*, 8(1):15–25, 2015.
- [27] Zotter, F., M. Frank. *Ambisonics: A practical 3D audio theory for recording, studio production, sound reinforcement, and virtual reality*. Springer Nature, 2019.
- [28] Liu, F., J. Kang. Relationship between street scale and subjective assessment of audio-visual environment comfort based on 3d virtual reality and dual-channel acoustic tests. *Building and Environment*, 129:35–45, 2018.
- [29] Huang, Y., J. Benesty, G. W. Elko, et al. Real-time passive source localization: A practical linear-correction least-squares approach. *IEEE transactions on Speech and Audio Processing*, 9(8):943–956, 2001.
- [30] Schmidt, R. Multiple emitter location and signal parameter estimation. *IEEE Transactions on Antennas and Propagation*, 34(3):276–280, 1986.
- [31] Liu, W., S. Weiss. *Wideband beamforming: concepts and techniques*. John Wiley & Sons, 2010.
- [32] Heymann, J., L. Drude, R. Haeb-Umbach. Neural network based spectral mask estimation for acoustic beamforming. In *2016 IEEE International Conference on Acoustics, Speech and Signal Processing (ICASSP)*, pages 196–200. IEEE, 2016.
- [33] Habets, E. A. P., J. Benesty, I. Cohen, et al. New insights into the mvdr beamformer in room acoustics. *IEEE Transactions on Audio, Speech, and Language Processing*, 18(1):158–170, 2009.
- [34] Wang, D., J. Chen. Supervised speech separation based on deep learning: An overview. *IEEE/ACM Transactions on Audio, Speech, and Language Processing*, 26(10):1702–1726, 2018.
- [35] Huang, P.-S., M. Kim, M. Hasegawa-Johnson, et al. Joint optimization of masks and deep recurrent neural networks for monaural source separation. *IEEE/ACM Transactions on Audio, Speech, and Language Processing*, 23(12):2136–2147, 2015.

- [36] Drude, L., D. Hasenklever, R. Haeb-Umbach. Unsupervised training of a deep clustering model for multichannel blind source separation. In *IEEE International Conference on Acoustics, Speech and Signal Processing (ICASSP)*, pages 695–699. 2019.
- [37] Wisdom, S., E. Tzinis, H. Erdogan, et al. Unsupervised sound separation using mixture invariant training. *Advances in Neural Information Processing Systems*, 33:3846–3857, 2020.
- [38] Hu, K., D. Wang. An unsupervised approach to cochannel speech separation. *IEEE Transactions on audio, speech, and language processing*, 21(1):122–131, 2012.
- [39] Gerzon, M. A. Periphony: With-height sound reproduction. *Journal of the audio engineering society*, 21(1):2–10, 1973.
- [40] Furness, R. K. Ambisonics-an overview. In *Audio Engineering Society Conference: 8th International Conference: The Sound of Audio*. Audio Engineering Society, 1990.
- [41] Frank, M., F. Zotter, A. Sontacchi. Producing 3d audio in ambisonics. In *Audio Engineering Society Conference: 57th International Conference: The Future of Audio Entertainment Technology—Cinema, Television and the Internet*. Audio Engineering Society, 2015.
- [42] Daniel, J., S. Moreau. Further study of sound field coding with higher order ambisonics. In *Audio Engineering Society Convention 116*. Audio Engineering Society, 2004.
- [43] Moreau, S., J. Daniel, S. Bertet. 3d sound field recording with higher order ambisonics—objective measurements and validation of a 4th order spherical microphone. In *120th Convention of the AES*, pages 20–23. 2006.
- [44] Adavanne, S., A. Politis, T. Virtanen. Direction of arrival estimation for multiple sound sources using convolutional recurrent neural network. In *IEEE European Signal Processing Conference (EUSIPCO)*, pages 1462–1466. 2018.
- [45] Mildenhall, B., P. P. Srinivasan, M. Tancik, et al. Nerf: Representing scenes as neural radiance fields for view synthesis. In *European conference on computer vision*, pages 405–421. Springer, 2020.
- [46] Waibel, A., T. Hanazawa, G. Hinton, et al. Phoneme recognition using time-delay neural networks. *IEEE Transactions on Acoustics, Speech, and Signal Processing*, 37(3):328–339, 1989.
- [47] Ioffe, S., C. Szegedy. Batch normalization: Accelerating deep network training by reducing internal covariate shift. In *International Conference on Machine Learning*, pages 448–456. PMLR, 2015.
- [48] Brownlee, J. A gentle introduction to the rectified linear unit (relu). *Machine Learning Mastery*, 6, 2019.
- [49] Chung, J., C. Gulcehre, K. Cho, et al. Empirical evaluation of gated recurrent neural networks on sequence modeling. *Conference on Neural Information Processing Systems*, 2014.
- [50] Narayanan, A., D. Wang. Ideal ratio mask estimation using deep neural networks for robust speech recognition. In *IEEE International Conference on Acoustics, Speech and Signal Processing*, pages 7092–7096. 2013.
- [51] Yamagishi, J., C. Veaux, K. MacDonald, et al. Cstr vctk corpus: English multi-speaker corpus for cstr voice cloning toolkit (version 0.92). 2019.
- [52] Rafii, Z., A. Liutkus, F.-R. Stöter, et al. Musdb18-a corpus for music separation. 2017.
- [53] Trowitzsch, I., J. Taghia, Y. Kashef, et al. The nigen general sound events database. *arXiv preprint arXiv:1902.08314*, 2019.
- [54] Kingma, D. P., J. Ba. Adam: A method for stochastic optimization. In *International Conference for Learning Representations (ICLR)*. 2015.